Quaternion-based I&I Robust Adaptive SMC for Multirotor UAVs

J. U. Alvarez-Munoz[1,2], J. Escareno[3], J. Gustave[1], O. Labbani-Igbida[3]

***Abstract*— This work presents a novel adaptive control architecture for vertical take-off and landing (VTOL) vehicles to reduce reliance on model-based knowledge. To accomplish trajectory-tracking tasks, we first merge the recursive stability of Backstepping with the robustness of sliding-mode control (SMC) laws. Additionally, an Immersion & Invariance (I&I)-based update law drives the error estimation to an invariant manifold for enhanced disturbance rejection. Subsequently, relying entirely on the quaternion representation for dynamics modeling, we detail an adaptive I&I control law for attitude stabilization. Closed-loop stability is proven by means of Lyapunov's theory. Finally, the overall strategy is assessed through numerical simulations of a unmanned aerial vehicle (UAV) performing a trajectory-tracking mission exposed to a limited-knowledge model and unknown disturbances.**

I. INTRODUCTION

Unmanned Aerial Vehicles (UAVs) have become indispensable tools in civil, industrial, and defense applications, including inspection, mapping, surveillance, and autonomous navigation. Multirotor Vertical Take-Off and Landing (VTOL) platforms, in particular, offer high maneuverability, mechanical simplicity, and the ability to operate in cluttered environments. However, these vehicles are inherently nonlinear and under-actuated, and their performance is strongly affected by parametric uncertainties, unmodeled dynamics, and time-varying disturbances. Ensuring reliable operation under such conditions requires control strategies that go beyond classical linear approaches [1].

Linear controllers such as PID and LQR remain widely used due to their simplicity and ease of implementation [2], [3]. Nevertheless, their effectiveness is restricted to a narrow operating region, and their robustness degrades significantly when the system deviates from nominal conditions or when aerodynamic parameters vary during flight. To address these limitations, numerous nonlinear control strategies, such as backstepping, sliding mode control (SMC) or adaptive variants of these methods have been proposed, [4], [5]. Backstepping has been extensively applied to multirotor stabilization due to its recursive structure and its ability to handle strict-feedback dynamics [4], while SMC is well known for its inherent robustness against matched disturbances and modeling errors [5]–[7]. Adaptive extensions of these controllers have also been developed to compensate for unknown parameters or external perturbations [8], although they may introduce chattering or require accurate model structures.

A sophisticated alternative for an adaptive method is the I&I framework, proposed in [9]. By immersing the system into a lower-order stable target system, it ensures that estimates converge on an invariant manifold. Its advantages for the control of VTOL systems have been presented in [10].

Despite these advances, many existing works rely on Euler-angle parametrizations, which suffer from singularities. In this sense, quaternion-based formulations provide a globally valid alternative and have been successfully employed in geometric and nonlinear control frameworks [11], [12]. However, fully quaternion-based nonlinear adaptive controllers remain relatively scarce, especially featuring hybrid robust–adaptive properties.

In this context, this work proposes a full-quaternion inner-outer loop architecture for a rotorcraft UAV, integrating adaptive I&I principles for both subsystems. First, the position controller adopts a backstepping methodology to exploit the natural cascade structure of the translational dynamics. To enhance disturbance robustness, reduce precise model dependency, and mitigate typical SMC chattering, a sliding mode term is hybridized with an adaptive I&I formulation, yielding a disturbance-resilient, switching-free controller. Second, an inner adaptive I&I attitude control law is formulated using unit-quaternions. This compensates for unknown parameters and time-varying disturbances while avoiding Euler angle singularities, ensuring globally valid attitude control. To our knowledge, simultaneously integrating a full-quaternion formulation, adaptive I&I principles, and a backstepping-SMC hybrid strategy addresses a gap in current nonlinear UAV control literature.

The effectiveness of the proposed control laws is demonstrated through a rigorous stability analysis and a detailed simulation involving stabilization and trajectory tracking of a UAV under unknown and time-varying disturbances.

The remainder of the paper is organized as follows. Section II presents some theory related to quaternions. Section III describes the dynamic model of the rotorcraft. The robust backstepping–SMC–I&I position controller and the adaptive I&I attitude controller are explained in Section IV. Section V reports simulation results validating the proposed approach. Section VI concludes the paper and outlines future research directions.

II. THEORETICAL PRELIMINARIES

A. Unit Quaternion Representation

Consider a body fixed, main coordinate frame with the orthonormal right handed basis $B(x_b, y_b, z_b)$, and an inertial frame with basis $N(x_n, y_n, z_n)$, see Fig. 1. The rotation of B w.r.t. N can be parameterized in terms of a rotation $\beta \in \mathbb{R}$

[1] Institut Polytechnique de Sciences Avancées, 94200, Ivry-sur-Seine, France. jonatan.alvarez@ipsa.fr

[2] Laboratoire Images, Signaux et Systèmes Intelligents (LISSI), Université Paris-Est Créteil (UPEC), 94400 Vitry-sur-Seine, France.

[3] Robotics and Mechatronics Department, XLIM Research Institute UMR-CNRS, 87060, University of Limoges, France.

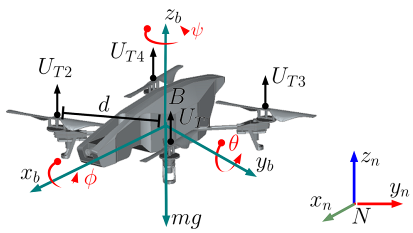

Fig. 1: Free-body scheme: VTOL rotorcraft

about a fixed axis $\boldsymbol{e}_\nu \in \mathbb{S}^2 \subset \mathbb{R}^3$ by the map $\mathcal{U} : \mathbb{R} \times \mathbb{S}^2 \to SO(3)$, defined as

$$\mathcal{U}(\beta, \boldsymbol{e}_\nu) = I_3 + \sin\beta[\boldsymbol{e}_\nu^\times] + (1 - \cos\beta)[\boldsymbol{e}_\nu^\times]^2 \tag{1}$$

where $I_3 \in \mathbb{R}^{3\times3}$ is the identity matrix and $[^\times]$ is used to map a vector to a skew-symmetric matrix. Therefore, a unit quaternion $q \in \mathbb{S}^3 \subset \mathbb{R}^4$, is defined as:

$$\boldsymbol{q} := \left(\cos\beta/2, \boldsymbol{e}_\nu \sin\beta/2\right)^T = \left(q_0, \boldsymbol{q}_v^T\right)^T \tag{2}$$

where $\boldsymbol{q}_v = (q_1, q_2, q_3)^T \in \mathbb{R}^3$ and $q_0 \in \mathbb{R}$ are known as the vector and scalar parts of the quaternion, respectively.

Let $\boldsymbol{\omega} = (\omega_1, \omega_2, \omega_3)^T$ be the angular velocity vector of the body coordinate frame B, relative to the inertial coordinate frame N, the kinematics equation is given by

$$\begin{pmatrix} \dot{q}_0 \\ \dot{\boldsymbol{q}}_v \end{pmatrix} = \frac{1}{2} \begin{pmatrix} -\boldsymbol{q}_v^T \\ I_3 q_0 + [\boldsymbol{q}_v^\times] \end{pmatrix} \boldsymbol{\omega} = \frac{1}{2}\Xi(\boldsymbol{q})\boldsymbol{\omega} \tag{3}$$

A rotation matrix $R(\boldsymbol{q})$ related to the unit quaternion $\boldsymbol{q}$, allowing to rotate a vector from B to N, can be written as:

$$R(\boldsymbol{q}) = (q_0^2 - \boldsymbol{q}_v^T\boldsymbol{q}_v)I_3 + 2\boldsymbol{q}_v\boldsymbol{q}_v^T + 2q_0[\boldsymbol{q}_v^\times] \tag{4}$$

Given a desired quaternion $\boldsymbol{q}_d$ and an actual quaternion $\boldsymbol{q}$, $\boldsymbol{q}_e$ is the quaternion error, computed as the quaternion multiplication of the conjugate of the desired quaternion $\boldsymbol{q}_d$ and $\boldsymbol{q}$:

$$\tilde{\boldsymbol{q}} := \boldsymbol{q}_d^\star \otimes \boldsymbol{q} = (\tilde{q}_0, \tilde{\boldsymbol{q}}_v{}^T)^T \tag{5}$$

where $\otimes$ denotes the quaternion multiplication and $\boldsymbol{q}_d^\star = (q_{0d}, -\boldsymbol{q}_v^T)^T$.

III. Mathematical Modelling

An aerial system can be modeled as a rigid body, see Fig. 1. Then, the six degrees of freedom model (position and orientation) of the system, considering the quaternion representation, can be separated into translational and rotational motions, defined by

$$\Sigma_T : \begin{cases} \dot{\boldsymbol{p}} = \boldsymbol{v} \\ \dot{\boldsymbol{v}} = -g\boldsymbol{e}_3 + \frac{U_T}{m}R(\boldsymbol{q})\boldsymbol{e}_3 - \frac{K_{dT}}{m}\boldsymbol{v} + \frac{\boldsymbol{d}_T}{m} \end{cases} \tag{6}$$

$$\Sigma_R : \begin{cases} \dot{\boldsymbol{q}} = \frac{1}{2}\Xi(\boldsymbol{q})\boldsymbol{\omega} \\ J\dot{\boldsymbol{\omega}} = -\boldsymbol{\omega}^\times J\boldsymbol{\omega} + \boldsymbol{\Gamma} - lK_{dR}\boldsymbol{w} + \boldsymbol{d}_R \end{cases} \tag{7}$$

where $\boldsymbol{p}$ and $\boldsymbol{v} \in \mathbb{R}^3$ are linear positions and velocities in the inertial frame, m is the mass of the aerial system, g is the gravity acceleration, $\boldsymbol{e}_3 \in \mathbb{R}^3$ is a unitary vector along the z axis, $R(\boldsymbol{q})$ is the rotation matrix given in (4), $U_T \in \mathbb{R}$ is the total thrust generated by the four rotors and $\boldsymbol{d}_T \in \mathbb{R}^3$ corresponds to a disturbance, bounded as $\|\boldsymbol{d}_T\| \leq \boldsymbol{d}_{Tmax}$. $J \in \mathbb{R}^{3\times3}$ is the inertia matrix, $\boldsymbol{\Gamma} \in \mathbb{R}^3$ is the vector of applied torques and $\boldsymbol{d}_R \in \mathbb{R}^3$ stands for time-varying external disturbances, such that $\|\boldsymbol{d}_R\| \leq \boldsymbol{d}_{Rmax}$. Finally, $K_{dt}, K_{dR} \in \mathbb{R}^{3\times3}$ are drag coefficients and l is the quadrotor radius.

IV. Control Design

This section presents two control strategies: the position and attitude control laws. The first one is synthesized to achieve trajectory-tracking objectives under unknown time-varying disturbances. Then, the attitude controller ensures attitude stabilization of the multi rotor system.

A. Position Control Strategy for the VTOL System

Let the VTOL system dynamics (6) be rewritten as

$$\Sigma_T : \begin{cases} \dot{\boldsymbol{p}} = \boldsymbol{v} \\ \dot{\boldsymbol{v}} = -g\boldsymbol{e}_3 + \boldsymbol{u}_p + \frac{K_{dT}}{m}\boldsymbol{v} + \frac{\boldsymbol{d}_T}{m} \end{cases} \tag{8}$$

where $\boldsymbol{u}_p = \frac{U_T}{m}R(\boldsymbol{q})\boldsymbol{e}_3$. Now, let two variable errors $\boldsymbol{e}_{1T} \in \mathbb{R}^3$ and $\boldsymbol{e}_{2T} \in \mathbb{R}^3$ with their respective time derivatives be expressed as

$$\begin{aligned} \boldsymbol{e}_{1T} &= \boldsymbol{p} - \boldsymbol{p}_d \\ \boldsymbol{e}_{2T} &= \dot{\boldsymbol{e}}_{1T} + \rho\boldsymbol{e}_{1T} \end{aligned} \tag{9}$$

$$\begin{aligned} \dot{\boldsymbol{e}}_{1T} &= \boldsymbol{e}_{2T} - \rho\boldsymbol{e}_{1T} \\ \dot{\boldsymbol{e}}_{2T} &= -g\boldsymbol{e}_3 + \boldsymbol{u}_p + \boldsymbol{\Delta}_T - \dot{\boldsymbol{v}}_d - \rho\dot{\boldsymbol{e}}_{1T} \end{aligned} \tag{10}$$

such that $\boldsymbol{e}_{2T}$ denotes the filtered position tracking error and $\rho > 0 \in \mathbb{R}^{3\times3}$ is a diagonal constant matrix. Furthermore, $\boldsymbol{\Delta}_T = -\frac{K_{dT}\boldsymbol{v}}{m} + \frac{\boldsymbol{d}_T}{m}$ and $\boldsymbol{e}_T = (\boldsymbol{e}_{1T}^T, \boldsymbol{e}_{2T}^T)^T$. With this, an error manifold $\boldsymbol{z}_T \in \mathbb{R}^3$ is defined as

$$\boldsymbol{z}_T = \hat{\boldsymbol{\Delta}}_T - \boldsymbol{\Delta}_T + \boldsymbol{\beta}_T \tag{11}$$

where $\hat{\boldsymbol{\Delta}}_T = (\hat{\Delta}_{1T}, \hat{\Delta}_{2T}, \hat{\Delta}_{3T})^T \in \mathbb{R}^3$ is the estimate of $\boldsymbol{\Delta}_T$ and $\boldsymbol{\beta}_T = (\beta_1(\boldsymbol{e}_T), \beta_2(\boldsymbol{e}_T), \beta_3(\boldsymbol{e}_T))^T \in \mathbb{R}^3$ is a correction function. Assuming a nominally slowly-varying disturbance ($\dot{\boldsymbol{\Delta}}_T \approx \boldsymbol{0}$) for the estimator design, the time derivative of (11) reads as

$$\begin{aligned} \dot{\boldsymbol{z}}_T =& \dot{\hat{\boldsymbol{\Delta}}}_T + \frac{\partial\beta_T}{\partial\boldsymbol{e}_{1T}^T}\dot{\boldsymbol{e}}_{1T} + \frac{\partial\beta_T}{\partial\boldsymbol{e}_{2T}^T}(-g\boldsymbol{e}_3 + \boldsymbol{u}_p + \boldsymbol{\Delta}_T - \dot{\boldsymbol{v}}_d \\ &- \rho\dot{\boldsymbol{e}}_{1T}) \end{aligned} \tag{12}$$

where $\boldsymbol{\Delta}_T = \hat{\boldsymbol{\Delta}}_T + \boldsymbol{\beta}_T - \boldsymbol{z}_T$. Thus, based on (12), the adaptive law $\dot{\hat{\Delta}}_T$ and the correction function $\boldsymbol{\beta}_T$ are synthesized as

$$\begin{aligned} \dot{\hat{\boldsymbol{\Delta}}}_T =& -\frac{\partial\boldsymbol{\beta}_T}{\partial\boldsymbol{e}_{1T}^T}\dot{\boldsymbol{e}}_{1T} - \frac{\partial\boldsymbol{\beta}_T}{\partial\boldsymbol{e}_{2T}^T}(-g\boldsymbol{e}_3 + \boldsymbol{u}_p + \boldsymbol{\Delta}_{eT} - \dot{\boldsymbol{v}}_d \\ &- \rho\dot{\boldsymbol{e}}_{1T}) \end{aligned} \tag{13}$$

$$\boldsymbol{\beta}_T = \int_0^{\boldsymbol{e}_{2T}} \lambda_T d\boldsymbol{e}_{2T} \tag{14}$$

where $\boldsymbol{\Delta}_{eT} = \hat{\boldsymbol{\Delta}}_T + \boldsymbol{\beta}_T$ and $\lambda_T \in \mathbb{R}^{3\times3}$ is a tuning diagonal matrix. Then, substituting (13) and (14) in (12), renders this one as

$$\dot{\boldsymbol{z}}_T = -\lambda_T\boldsymbol{z}_T \tag{15}$$

Now, in order to design the control law, let us adopt the backstepping methodology.

Step 1: By recalling (9), let a CLF related to e_{1T} and its time derivative be given as

$$V(e_{1T}) = \frac{1}{2} e_{1T}^T e_{1T} \quad (16)$$

$$\dot{V}(e_{1T}) = e_{1T}^T e_{2T} \quad (17)$$

Then, a virtual controller for e_{2T} is chosen as

$$e_{2T} = -\gamma e_{1T} \quad (18)$$

where $\gamma > 0 \in \mathbb{R}^{3\times3}$ is a diagonal constant matrix. Then, by substituting the latter in (17) yields $\dot{V}(e_{1T}) = -e_{1T}^T \gamma e_{1T} \leq 0$. Thus e_{1T} is stable and asymptotically convergent to the origin.

In the subsequent analyses, the following properties have been considered

- P1. $x^T x = \sum_{i=1}^n x_i^2 = \|x\|_2^2$
- P2. $\|x\|_2 \leq \|x\|_1$
- P3. $\|x\|_1 = \sum_{i=1}^n |x_i|$
- P4. $|x_i| = x^T \text{sign}(x)$
- P5. $x^T y \leq \frac{\|x\|^2}{2} + \frac{\|y\|^2}{2}$

for any vectors x and y with length equal no n.

Step 2: Let an error variable be defined as $s = (s_{px}, s_{py}, s_{pz})^T \in \mathbb{R}^3$. Then, considering (18) as a reference, i.e. $e_{d2T} = -\gamma e_{1T}$, allows to express s as

$$s = e_{2T} - e_{d2T} = e_{2T} + \gamma e_{1T} \quad (19)$$

Hence, the time derivative of (19) considering (10) is

$$\dot{s} = -g e_3 + u_p + \Delta_T - \dot{v}_d - \rho \dot{e}_{1T} + \gamma e_{2T} \quad (20)$$

In order to design the control strategy, let the next CLF and its time derivative be expressed by

$$V = \frac{1}{2} e_{1T}^T e_{1T} + \frac{1}{2} s^T s + \frac{1}{2} z_T^T \lambda_T^{-1} z_T \quad (21)$$

$$\begin{aligned} \dot{V} = &\, e_{1T} s - e_{1T}^T \gamma e_{1T} + s^T(-g e_3 + u_p + \Delta_T - \dot{v}_d \\ & - \rho \dot{e}_{1T} + \gamma e_{2T}) - z_T^T \dot{z}_T \end{aligned} \quad (22)$$

To guarantee $s = \dot{s} = 0$, the control input u_p is composed of the equivalent u_{eq} and the switching u_{sw} control components. Then, according to (22) the control law is designed as follows

$$\begin{aligned} u_p = &\underbrace{g e_3 + \dot{v}_d - \hat{\Delta}_{eT} - (\rho^2 + I_3) e_{1T} - (\gamma - \rho) e_{2T}}_{u_{eq}} \\ & \underbrace{-Q_1 \text{sign}(s) - Q_2 s}_{u_{sw}} \end{aligned} \quad (23)$$

where $\hat{\Delta}_{eT} = \hat{\Delta}_T + \beta_T$. Likewise, $Q_1 > 0, Q_2 > 0 \in \mathbb{R}^{3\times3}$ are constant diagonal matrices and $\text{sign}(s) = (\text{sign}(s_{px}), \text{sign}(s_{py}), \text{sign}(s_{pz}))^T \in \mathbb{R}^3$. Then, by inserting the control strategy (23) in (22) yields

$$\begin{aligned} \dot{V} &= -e_{1T}^T \gamma e_{1T} - s^T Q_1 \text{sign}(s) - s^T Q_2 s - z_T^T z_T \\ &\leq -\lambda_{min}\{\gamma\} \|e_{1T}\|_2^2 - Q_1 \|s\|_1 - \lambda_{min}\{Q_2\} \|s\|_2^2 - \|z\|_2^2 \end{aligned} \quad (24)$$

where P1-P4 have been applied. Hence, provided that all terms on the right-hand side are negative implies that $\dot{V} \leq 0$, demonstrating asymptotic stability.

Remark 4.1: For implementation purposes, the set (13,14,23) is rewritten as

$$\dot{\hat{\Delta}}_T = -\lambda_T(-g e_3 + u_p + \hat{\Delta}_T + \lambda_T d e_{2T} - \dot{v}_d - \rho \dot{e}_{1T}) \quad (25)$$

$$\beta_T = \lambda_T e_{2T} \quad (26)$$

$$\begin{aligned} u_p = &\, g e_3 + \dot{v}_d - \hat{\Delta}_T - \lambda_T e_{2T} - (\rho^2 + I_3) e_{1T} \\ & - (\gamma - \rho) e_{2T} - Q_1 \text{sign}(s) - Q_2 s \end{aligned} \quad (27)$$

Remark 4.2: By tuning the switching gain $Q_1 > \|\dot{\Delta}_T\|$, robustly rejects the unmodeled disturbance derivative. Furthermore, to eliminate chattering, the $\text{sign}(s)$ term is implemented via a continuous boundary-layer approximation $\tanh(s/\alpha)$. Together, these design choices guarantee practical sliding mode, confining the residual tracking errors to a compact neighborhood around the origin.

B. Reference Generation for the Attitude Controller

The position control strategy (23) can be used to generate the desired quaternion q_d for the attitude control law. Thus, inspired by the method in [12], the main goal is to define a desired rotation matrix as

$$R_d = (x_{b_d}^T, y_{b_d}^T, z_{b_d}^T)^T \quad (28)$$

where $R_d \in \mathbb{R}^{3\times3}$, and $x_{b_d}^T, y_{b_d}^T, z_{b_d}^T \in \mathbb{R}^3$ are desired directions for the body-fixed axes, such that

$$z_{b_d}^T = u_p / U_T \quad (29)$$

where u_p is the controller (23) and $U_T = m\|u_p\|$. Furthermore,

$$y_{b_d}^T = \frac{z_{b_d}^T \times \psi_{b_d}^T}{\|z_{b_d}^T \times \psi_{b_d}^T\|} \quad (30)$$

$$x_{b_d}^T = y_{b_d}^T \times z_{b_d}^T \quad (31)$$

where $\psi_{b_d}^T = (\cos\psi_d, \sin\psi_d, 0)^T \in \mathbb{R}^3$ with ψ_d the desired heading angle for the aerial system. Hence, in order to obtain q_d from R_d, it is possible to apply the methodology in [13]. To avoid singularities in (30), we assume standard flight avoiding free-fall ($U_T \neq 0$) and extreme horizontal thrust ($90°$ tilt), guaranteeing $z_{b_d}^T \times \psi_{b_d}^T \neq \mathbf{0}$.

C. Attitude Control Design

The attitude controller is intended to ensure attitude stabilization of the aerial vehicle, i.e. to the asymptotic conditions $\tilde{q} \to (1, \mathbf{0}^T)^T$, $\omega \to 0$ as $t \to \infty$. While stabilizing $\tilde{q}_v \to \mathbf{0}$ guarantees convergence to one of two equilibria that physically represent the same orientation in $SO(3)$, this can lead to the unwinding phenomenon. To achieve Almost Global Asymptotic Stability (AGAS) and prevent unwinding, the initial error is restricted to the hemisphere $\tilde{q}_0(0) > 0$, ensuring convergence to the unique equilibrium $+1$. For our case study, it is assumed that q_d is constant. Taking the time derivative of the error quaternion given in (5), the attitude kinematic error is

$$\dot{\tilde{q}}_v = T(\tilde{q}) \omega \quad (32)$$

where $T(\tilde{q}) = \frac{1}{2}(I_3 \tilde{q}_0 + [\tilde{q}_v^\times])$. To stabilize the kinematics, we design a virtual velocity controller as $\omega_r = -\alpha \tilde{q}_v$, where $\alpha >$

$0 \in \mathbb{R}$ a constant tuning parameter. Accordingly, we define the tracking error variables $\boldsymbol{e}_{1R} = (e_{11R}, e_{12R}, e_{13R})^T \in \mathbb{R}^3$ and $\boldsymbol{e}_{2R} = (e_{21R}, e_{22R}, e_{23R})^T \in \mathbb{R}^3$ as

$$\begin{aligned} \boldsymbol{e}_{1R} &= \tilde{\boldsymbol{q}}_v \\ \boldsymbol{e}_{2R} &= \boldsymbol{w} - \boldsymbol{w}_r = \boldsymbol{w} + \alpha \tilde{\boldsymbol{q}}_v \end{aligned} \tag{33}$$

where $\boldsymbol{e}_{2R}$ is the filtered tracking error. By using the quaternion kinematics (32) and considering (7), the time derivative of (33) is computed as

$$\begin{aligned} \dot{\boldsymbol{e}}_{1R} &= T(\tilde{\boldsymbol{q}})(\boldsymbol{e}_{2R} - \alpha \boldsymbol{e}_{1R}) \\ \dot{\boldsymbol{e}}_{2R} &= J^{-1}(-\boldsymbol{\omega}^\times J \boldsymbol{\omega} + \boldsymbol{\Gamma} + \boldsymbol{\Delta}_R) + \alpha \dot{\tilde{\boldsymbol{q}}}_v \end{aligned} \tag{34}$$

where $\boldsymbol{e}_R = (\boldsymbol{e}_{1R}^T, \boldsymbol{e}_{2R}^T)^T$ and $\boldsymbol{\Delta}_R = -l K_{dr} \boldsymbol{w} + \boldsymbol{d}_R$. Now, let an error manifold $\boldsymbol{z}_R = (z_{1R}, z_{2R}, z_{3R})^T \in \mathbb{R}^3$ be defined as

$$\boldsymbol{z}_R = \hat{\boldsymbol{\Delta}}_R - \boldsymbol{\Delta}_R + \boldsymbol{\beta}_R \tag{35}$$

where $\hat{\boldsymbol{\Delta}}_R = (\hat{\Delta}_{1R}, \hat{\Delta}_{2R}, \hat{\Delta}_{3R})^T \in \mathbb{R}^3$ is the online estimation of $\boldsymbol{\Delta}_R$ and $\boldsymbol{\beta}_R = (\beta_1(\boldsymbol{e}_R), \beta_2(\boldsymbol{e}_R), \beta_3(\boldsymbol{e}_R))^T \in \mathbb{R}^3$ is a correction function designed later.

Assumption 4.3: The disturbance $\boldsymbol{\Delta}_R$ is slowly varying relative to the attitude dynamics, implying $\dot{\boldsymbol{\Delta}}_R \approx \mathbf{0}$.

By finding the time derivative of (35), we obtain

$$\begin{aligned} \dot{\boldsymbol{z}}_R =& \dot{\hat{\boldsymbol{\Delta}}}_R + \frac{\partial \beta_R}{\partial \boldsymbol{e}_{1R}^T} \dot{\boldsymbol{e}}_{1R} + \frac{\partial \beta_R}{\partial \boldsymbol{e}_{2R}^T} (J^{-1}(-\boldsymbol{w}^\times J \boldsymbol{w} + \boldsymbol{\Gamma} + \boldsymbol{\Delta}_R) \\ &+ \alpha \dot{\tilde{\boldsymbol{q}}}_v) \end{aligned} \tag{36}$$

where $\boldsymbol{\Delta}_R = \hat{\boldsymbol{\Delta}}_R + \boldsymbol{\beta}_R - \boldsymbol{z}_R$. By applying Assumption 4.3 and seeking to express the latter as

$$\dot{\boldsymbol{z}}_R = -\lambda_R \boldsymbol{z}_R \tag{37}$$

we select the adaptive update law $\dot{\hat{\Delta}}_R$, the correction function β_R and the torque control input Γ as follows

$$\dot{\hat{\boldsymbol{\Delta}}}_R = -\frac{\partial \boldsymbol{\beta}_R}{\partial \boldsymbol{e}_{1R}^T} \dot{\boldsymbol{e}}_{1R} - \frac{\partial \boldsymbol{\beta}_R}{\partial \boldsymbol{e}_{2R}^T} (J^{-1}(-\boldsymbol{w}^\times J \boldsymbol{w} + \boldsymbol{\Gamma} + \boldsymbol{\Delta}_{eR}) + \alpha \dot{\tilde{\boldsymbol{q}}}_v) \tag{38}$$

$$\boldsymbol{\beta}_R = \int_0^{\boldsymbol{e}_{2r}} \lambda_R J d\boldsymbol{e}_{2R} \tag{39}$$

$$\Gamma = \boldsymbol{w}^\times J \boldsymbol{w} - \boldsymbol{\Delta}_{eR} - J\left(\alpha T(\tilde{\boldsymbol{q}}) \boldsymbol{w} + K_{2R} \boldsymbol{e}_{2R}\right) - K_{1R} \boldsymbol{e}_{1R} \tag{40}$$

where $\boldsymbol{\Delta}_{eR} = \hat{\boldsymbol{\Delta}}_R + \beta_R$. Furthermore, $K_{1R} > 0 \in \mathbb{R}$ a scalar tuning parameter and $\lambda_R > 0, K_{2R} > 0 \in \mathbb{R}^{3\times 3}$ are constant tuning diagonal matrices. Now, by substituting (40) and (35) into (34), this one becomes into

$$\begin{aligned} \dot{\boldsymbol{e}}_{1R} &= T(\tilde{\boldsymbol{q}})(\boldsymbol{e}_{2R} - \alpha \boldsymbol{e}_{1R}) \\ \dot{\boldsymbol{e}}_{2R} &= -K_{2R} \boldsymbol{e}_{2R} - J^{-1} K_{1R} \boldsymbol{e}_{1R} - J^{-1} \boldsymbol{z}_R \end{aligned} \tag{41}$$

Theorem 4.4: Consider the closed-loop dynamics described in (37). If the adaptation law $\dot{\hat{\boldsymbol{\Delta}}}_R$, the correction function β_R and the control law $\boldsymbol{\Gamma}$ are respectively designed as in (38), (39) and (40), then the tracking-error $\boldsymbol{e}_R$ is almost globally asymptotically stabilized to the origin, i.e. $\boldsymbol{e}_R \to 0$ as $t \to \infty$.

Proof: Let a Candidate Lyapunov Function (CLF) be given as

$$V(\boldsymbol{z}_R) = \frac{1}{2} \boldsymbol{z}_R^T \lambda_R^{-1} \boldsymbol{z}_R \tag{42}$$

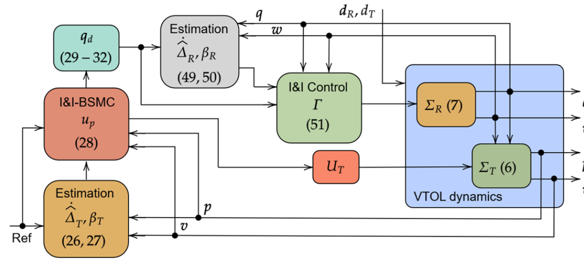

Fig. 2: Block diagram of the overall system

The time derivative of $V(\boldsymbol{z}_R)$ considering (37) yields

$$\dot{V}(\boldsymbol{z}_R) = \boldsymbol{z}_R^T \lambda_R^{-1} \dot{\boldsymbol{z}}_R = -\boldsymbol{z}_R^T \boldsymbol{z}_R = -2V(\boldsymbol{z}_R) \tag{43}$$

Hence, $\boldsymbol{z}_R$ converges exponentially. For full closed-loop stability, the composite CLF is:

$$\begin{aligned} V(\boldsymbol{e}_R, \boldsymbol{z}_R) &= K_{1R}((1 - \tilde{q}_0)^2 + \tilde{\boldsymbol{q}}_v^T \tilde{\boldsymbol{q}}_v) + \frac{1}{2} \boldsymbol{e}_{2R}^T J \boldsymbol{e}_{2R} + V(\boldsymbol{z}_R) \\ &= 2K_{1R}(1 - \tilde{q}_0) + \frac{1}{2} \boldsymbol{e}_{2R}^T J \boldsymbol{e}_{2R} + \frac{1}{2} \boldsymbol{z}_R^T \lambda_R^{-1} \boldsymbol{z}_R \end{aligned} \tag{44}$$

The time derivative of (44) considering (37) and (41) is computed as

$$\begin{aligned} \dot{V}(\boldsymbol{e}_R, \boldsymbol{z}_R) =& K_{1R} \boldsymbol{e}_{1R}^T (\boldsymbol{e}_{2R} - \alpha \boldsymbol{e}_{1R}) - \boldsymbol{e}_{2R}^T J K_{2R} \boldsymbol{e}_{2R} \\ &- \boldsymbol{e}_{2R}^T K_{1R} \boldsymbol{e}_{1R} - \boldsymbol{e}_{2R}^T \boldsymbol{z}_R - \boldsymbol{z}_R^T \boldsymbol{z}_R \\ \leq& - K_{1R} \alpha \|\boldsymbol{e}_{1R}\|_2^2 - \boldsymbol{e}_{2R}^T J K_{2R} \boldsymbol{e}_{2R} \\ &- \boldsymbol{e}_{2R}^T \boldsymbol{z}_R - \|\boldsymbol{z}_R\|^2 \end{aligned} \tag{45}$$

where we have used P1. Now, considering P5 yields

$$\begin{aligned} \dot{V}(\boldsymbol{e}_R, \boldsymbol{z}_R) \leq& - K_{1R} \alpha \|\boldsymbol{e}_{1R}\|_2^2 \\ &- \lambda_{min}\{J K_{2R} - \frac{1}{2} I_3\} \|\boldsymbol{e}_{2R}\|_2^2 - \frac{\|\boldsymbol{z}_R\|_2^2}{2} \end{aligned} \tag{46}$$

with $\lambda_{min}\{\cdot\}$ being the minimum eigenvalue. It follows that $\dot{V}(\boldsymbol{e}_R, \boldsymbol{z}_R) \leq 0$ if $J K_{2R} > \frac{1}{2} I_3$ ensuring AGAS, completing the proof. ■

Remark 4.5: To avoid numerical noise, the attitude reference is treated as quasi-static ($\boldsymbol{\omega}_d = \mathbf{0}$). The resulting unmodeled reference kinematics and time-varying disturbances ($\|\dot{\boldsymbol{\Delta}}_R\| \leq \delta_R$) act as bounded disturbances. This relaxes asymptotic stability to Uniform Ultimate Boundedness (UUB), where high-gain tuning keeps residual tracking errors negligibly small.

Remark 4.6: In order to implement the control law, the set (38-40) is rewritten as

$$\dot{\hat{\boldsymbol{\Delta}}}_R = -\lambda_R(-\boldsymbol{w}^\times J \boldsymbol{w} + \boldsymbol{\Gamma} + \hat{\boldsymbol{\Delta}}_R + \lambda_R J \boldsymbol{e}_{2R} + \alpha \dot{\tilde{\boldsymbol{q}}}_v) \tag{47}$$

$$\boldsymbol{\beta}_R = \lambda_R J \boldsymbol{e}_{2R} \tag{48}$$

$$\begin{aligned} \Gamma = \boldsymbol{w}^\times J \boldsymbol{w} - \hat{\boldsymbol{\Delta}}_R - \lambda_R J \boldsymbol{e}_{2R} - J(\alpha T(\tilde{\boldsymbol{q}}) \boldsymbol{w} \\ + K_{2R} \boldsymbol{e}_{2R}) - K_{1R} \boldsymbol{e}_{1R} \end{aligned} \tag{49}$$

An overview of the entire control architecture is presented in Fig. 2.

V. Simulation Results

To asses the proposed approach, the current section presents simulation results. This one considers a multi-rotor system performing a trajectory tracking mission under unknown and time varying disturbances.

A. Simulation Scenario and Results

The numerical simulation to validate the proposed control architecture was performed using the Matlab/Simulink® environment. The physical parameters of the multi-rotor and the parameters for the control laws are provided in Table I.

System	Description	Value	Units
Quadcopter	Mass (m)	650	g
	Distance (d)	20	cm
	Inertial moment x, y (J_ϕ, J_θ)	0.0075	$Kg \cdot m^2$
	Inertial moment z (J_ψ)	0.013	$Kg \cdot m^2$
Attitude controller	$\lambda_{r\phi,r\theta,r\psi}$	1	
	α	0.5	
	K_{1r}	6	
	$K_{2\phi,2\theta}$	45	
	$K_{2\psi}$	33	
Position controller	$\lambda_{Tx,Ty,Tz}$	1.2	
	$\rho_{x,y,z}$	0.1	
	$\gamma_{x,y,z}$	1.2	
	$Q_{1x,1y,1z}$	1.6	
	$Q_{2x,2y,2z}$	0.2	

TABLE I: VTOL system and control parameters

The initial conditions for the system are $(\phi_0, \theta_0, \psi_0)^T = (2°, -2°, -15°)^T$ and $\boldsymbol{p}_0 = (1, -2, 0)^T$m. Then, the vehicle is sent to the position $\boldsymbol{p}_d = (1, -1, 2)^T$m. At time $t = 30$s, it performs a trajectory-tracking task, which corresponds to a periodic 3D square: $\boldsymbol{p}_d(t) = \boldsymbol{C}_i + (\boldsymbol{C}_{i+1} - \boldsymbol{C}_i)s(\tau)$, where $t_r = \text{mod}(t - 30, 80)$, $i = \lfloor t_r/20 \rfloor + 1$, $\tau = \frac{t_r}{20} - i + 1$, and $s(\tau) = 10\tau^3 - 15\tau^4 + 6\tau^5$ is a $\mathcal{C}^2$ quintic profile. The vertices are defined as $\boldsymbol{C}_1 = (1, -1, 2)^T$, $\boldsymbol{C}_2 = (5, -1, 4)^T$, $\boldsymbol{C}_3 = (5, 3, 2)^T$, $\boldsymbol{C}_4 = (1, 3, 4)^T$, and $\boldsymbol{C}_5 \equiv \boldsymbol{C}_1$. Finally, at $t = 15$s, inaccurate physical parameters are provided to the controllers and unknown time-varying disturbances are generated, which are the consequence of the Dryden spectral wind model. The latter models turbulent fluctuations added to a static mean flow, see [6] for more details.

The generated wind profile and the tracking performance are reported in Fig. 3, where a comparison between the proposed strategy, a quaternion-based integral SMC (QISMC), a PID controller and a robust adaptive backstepping controller (RABC, [14]) is conducted. The results of such comparison are more evident in Fig. 4 and Fig. 5, which present the linear positions and velocities, respectively. The zoom-in-views permit to see how fast the proposed approach compensates for disturbances, as well as for system uncertainties through the adaptive I&I term. A clear example is shown by p_z in Fig. 4, where, in addition to the disturbances, an incorrect mass m is provided to the controller. Behavior of the adaptive term is depicted in Fig. 6, showing rapid adaptation to both, disturbances and uncertainties.

Pursuing with the comparison, Fig. 7 depicts the angular positions during the simulation. We can see that, by applying the proposed adaptive I&I controller, faster convergence is ensured. For example, in the case of ψ, it can be observed that for $t \in [0, 2]$s, faster convergence is ensured with our approach. Fig. 8, shows the torques Γ, as well as the total thrust U_T, applied to the system. It is shown how Γ generates a signal opposite to the disturbance in order to compensate for it. The superiority of the combined control techniques (47-49) and (25-27) is reaffirmed through the Table II, which presents the root mean square (RMS) errors during the simulation.

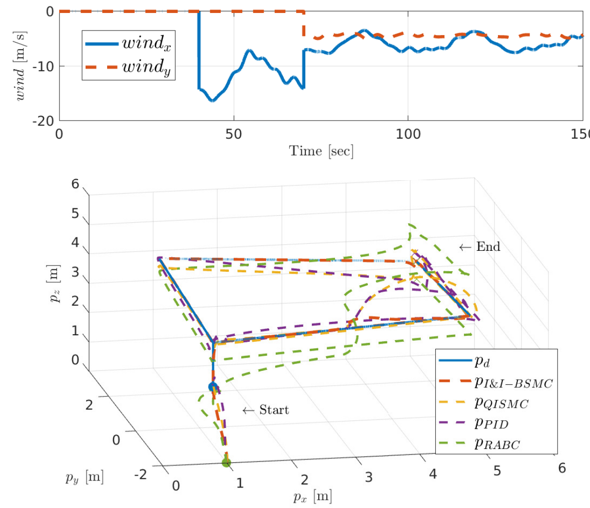

Fig. 3: Trajectory-tracking in 3D.

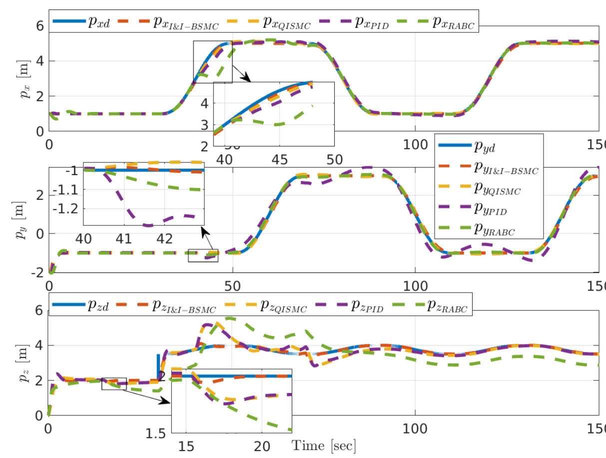

Fig. 4: Linear positions during the simulation

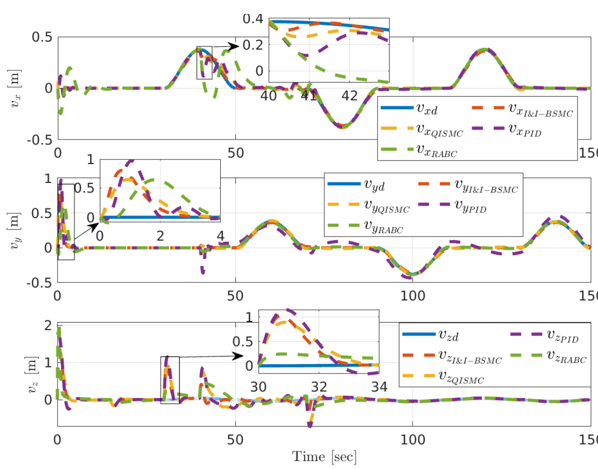

Fig. 5: Linear velocities during the simulation.

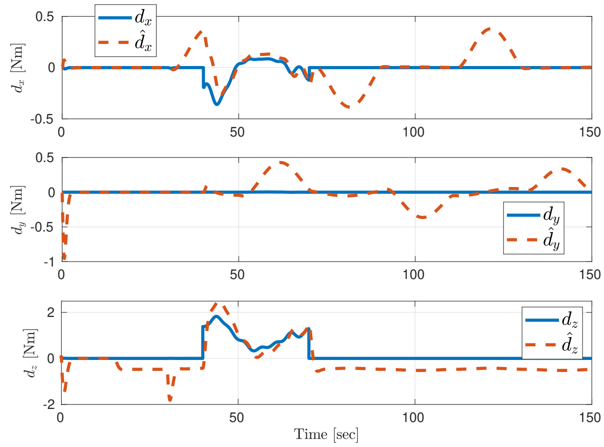

Fig. 6: Disturbance estimation during the simulation.

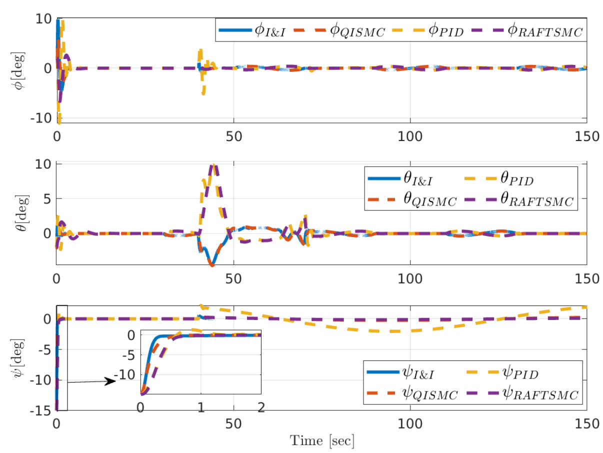

Fig. 7: Angular positions during the simulation.

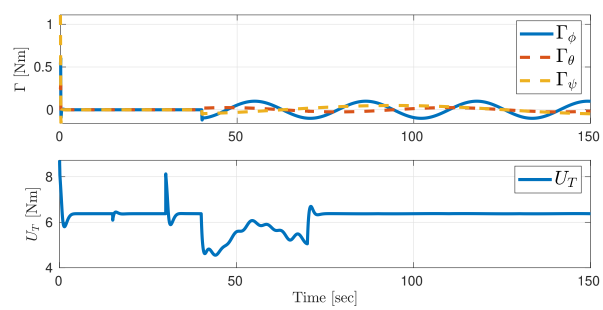

Fig. 8: Control signals for attitude and thrust.

Controller	RMS p_x m	RMS p_y m	RMS p_z	RMS $3D$
I&I-BSMC	0.0544	0.016	0.179	0.203
QISMC	0.23	0.046	0.585	0.628
PID	0.28	0.272	0.34	0.507
RABC [14]	0.868	0.112	0.857	1.225

TABLE II: RMS errors obtained during the simulation with the different controllers

VI. CONCLUSIONS

The present work detailed the synthesis of a novel robust adaptive control strategy for unmanned rotorcraft systems, designed to overcome model uncertainties and external disturbances. Merging I&I adaptation with a Backstepping-based SMC framework established a synergy balancing recursive stability, robustness, and smooth disturbance compensation. Moreover, quaternion formalism is used to derive the overall equations of motion, ensuring a singularity-free rotational representation. The controller's analytic viability is demonstrated via Lyapunov stability theory, and its effectiveness assessed through numerical simulations tracking a time-dependent trajectory under dynamic uncertainties. Results exhibited that the proposed controller outperforms conventional trajectory-tracking approaches in accuracy and disturbance rejection, rendering it a viable scheme for complex UAV missions in unpredictable environments. Forthcoming research includes experimental implementation and an extension to multi-agent systems control.

REFERENCES

[1] T. P. Nascimento and M. Saska, "Position and attitude control of multi-rotor aerial vehicles: A survey," *Annual Reviews in Control*, vol. 48, pp. 129–146, 2019.

[2] E. Paiva, J. Soto, J. Salinas, and W. Ipanaqué, "Modeling, simulation and implementation of a modified pid controller for stabilizing a quadcopter," in *2016 IEEE International Conference on Automatica (ICA-ACCA)*. IEEE, 2016, pp. 1–6.

[3] R. Guardeño, M. J. López, and V. M. Sánchez, "Mimo pid controller tuning method for quadrotor based on lqr/lqg theory," *Robotics*, vol. 8, no. 2, p. 36, 2019.

[4] N. Koksal, H. An, and B. Fidan, "Backstepping-based adaptive control of a quadrotor uav with guaranteed tracking performance," *ISA transactions*, vol. 105, pp. 98–110, 2020.

[5] J. J. Castillo-Zamora, K. A. Camarillo-Gomez, G. I. Perez-Soto, and J. Rodriguez-Resendiz, "Comparison of pd, pid and sliding-mode position controllers for v–tail quadcopter stability," *Ieee Access*, vol. 6, pp. 38 086–38 096, 2018.

[6] J. U. Alvarez-Munoz, J. A. Escareno, J. Chevalier, S. Daix, and O. Labanni-Igbida, "Wind-tolerant event-based adaptive sliding-mode control for vtol rotorcrafts multiagent systems," *IEEE Transactions on Aerospace and Electronic Systems*, vol. 59, no. 2, pp. 1400–1410, 2022.

[7] X. Wu, B. Xiao, and Y. Qu, "Modeling and sliding mode-based attitude tracking control of a quadrotor uav with time-varying mass," *ISA transactions*, vol. 124, pp. 436–443, 2022.

[8] Y. Zhang and J. Jiang, "Bibliographical review on reconfigurable fault-tolerant control systems," *Annual reviews in control*, vol. 32, no. 2, pp. 229–252, 2008.

[9] A. Astolfi and R. Ortega, "Immersion and invariance: A new tool for stabilization and adaptive control of nonlinear systems," *IEEE Transactions on Automatic control*, vol. 48, no. 4, pp. 590–606, 2003.

[10] B. Zhao, B. Xian, Y. Zhang, and X. Zhang, "Nonlinear robust adaptive tracking control of a quadrotor uav via immersion and invariance methodology," *IEEE Transactions on Industrial Electronics*, vol. 62, no. 5, pp. 2891–2902, 2014.

[11] A. Yazdanshenas and R. Faieghi, "Quaternion-based sliding mode control for six degrees of freedom flight control of quadrotors," in *2024 IEEE/RSJ International Conference on Intelligent Robots and Systems (IROS)*. IEEE, 2024, pp. 10 385–10 390.

[12] T. Lee, M. Leok, and N. H. McClamroch, "Geometric tracking control of a quadrotor uav on se (3)," in *49th IEEE conference on decision and control (CDC)*. IEEE, 2010, pp. 5420–5425.

[13] J. Diebel *et al.*, "Representing attitude: Euler angles, unit quaternions, and rotation vectors," *Stanford report*, vol. 58, no. 15-16, pp. 1–35, 2006.

[14] M. Labbadi and M. Cherkaoui, "Robust adaptive backstepping fast terminal sliding mode controller for uncertain quadrotor uav," *Aerospace Science and Technology*, vol. 93, p. 105306, 2019.